AIChE

Modeling of a Continuous Rotary Reactor for Carbon Nanotube Synthesis by Catalytic Chemical Vapor Deposition

Sophie L. Pirard and Jean-Paul Pirard
Institut de Chimie, Laboratoire de Génie Chimique, B6a, Université de Liège, B-4000 Liège, Belgium

Christophe Bossuot
Nanocyl S.A., Rue de l'Essor 4, B-5060 Sambreville, Belgium

DOI 10.1002/aic.11755
Published online January 22, 2009 in Wiley InterScience (www.interscience.wiley.com).

The modeling of carbon nanotube production by the CCVD process in a continuous rotary reactor with mobile bed was performed according to a rigorous chemical reaction engineering approach. The geometric, hydrodynamic, physical and physicochemical factors governing the process were analyzed in order to establish the reactor equations. While the study of the hydrodynamic factor suggests a co-current plug-flow approximation, the physical factor mainly deals with the phenomena of transport and the transfer of mass, which can be neglected. Concerning the physicochemical factor, the modeling is based on knowledge of the expression of the initial reaction rate, and takes into account catalytic deactivation as a function of time, according to a sigmoid decreasing law. The reactor modeling allows obtaining the evolution of partial pressure, carbon nanotube production and catalytic deactivation along the reactor for given initial operating conditions. The comparison between experimental and calculated production highlights a very good fit of data. © 2009 American Institute of Chemical Engineers *AIChE J,* 55: 675–686, 2009

Introduction

Carbon nanotubes represent a very promising new material, which has attracted much attention in the past few years. Intense research has been undertaken in order to identify the remarkable properties and potential applications of the nanotubes. Carbon nanotubes are now expected to bring significant breakthroughs in the technology of electronic and engineering materials.[1] The large-scale synthesis of nanotubes is the key point for their commercial application. Recently, several techniques such as electric arc-discharge, laser ablation, and catalytic chemical vapor deposition (CCVD),[1] have been successfully developed to synthesize carbon nanotubes. Although the first two methods can produce high-quality nanotubes in yields suitable for limited research use, they are not easily adaptable to industrial production, and the CCVD method appears to be the most promising for the processing of carbon nanotubes, due to its relatively low cost and its potential high-yield production.[2,3] Indeed, the CCVD method can be operated continuously and presents an advantage for large-scale production in comparison with other methods.

By using a discontinuous reactor, only a small quantity of carbon nanotubes from 0.01 to 0.2 kg can be produced daily by the CCVD process. It is for this reason that only a technology based on a continuous reactor can lead to the production of a large quantity of carbon nanotubes. Pilot-scale production reactors using the CCVD method are already running, and companies such as Arkema S.A., Bayer MaterialScience AG and Nanocyl S.A. are already present on the market, with an annual carbon nanotube production of over

Correspondence concerning this article should be addressed to S. L. Pirard at sophie.pirard@ulg.ac.be.

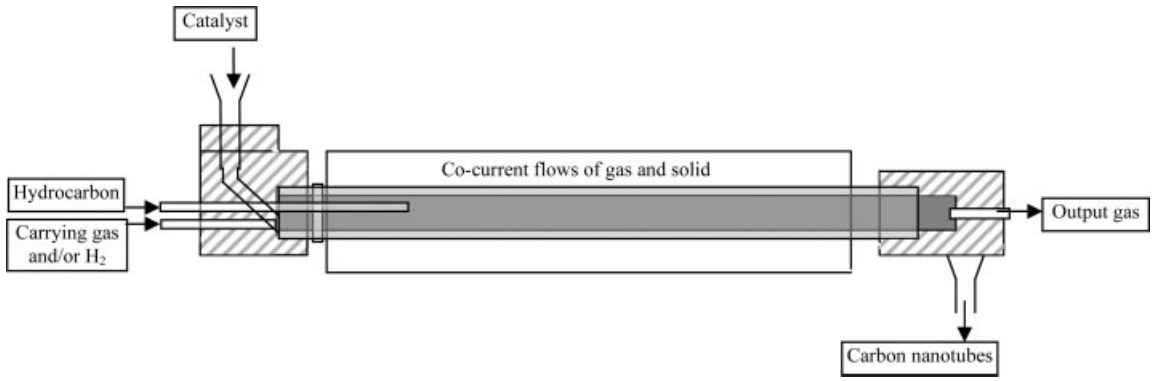

Figure 1. Schematic experimental setup.

10,000 kg.year^{-1}.[4–7] Other companies such as Hyperion, Iljin Nanotech and Shenzhen Nanotech Port are also leading multiwalled carbon nanotube producers, while Norman, South-West Nanotechnologies, Carbolex and Raymor Industries are active in single-walled carbon nanotube production.[7] Bayer and Arkema use a fluidized-bed process to produce carbon nanotubes.[7] This technology is easily scalable and allows a high carbon yield, a high-space-time yield, and a good mixing of the catalyst and of the produced carbon nanotubes. However, a fluidized bed also presents several drawbacks, such as a great variation of material density during the reaction, the cutting up of the catalytic support, and the breaking-up of carbon nanotubes due to great agitation. Nanocyl S.A. produces carbon nanotubes in a mobile-bed inclined rotating reactor.[8] This technology was chosen because the kinetics of carbon nanotube synthesis by hydrocarbon decomposition is quite slow, and because the ratio between the volume of product and of catalyst is very large (larger than 50). Furthermore, the rotation of the reactor allows the rolling of particles inside the reactor. So a good mixing of particles is possible during the reaction. Furthermore, the flow regime does not correspond to a heterogeneous phase between gas and solid, and it tends to be a homogeneous regime because of the best gas-solid contact.

The design and the development of a catalytic reactor require an integrated approach, according to chemical engineering methodology, which includes catalyst preparation and characterization, kinetic studies and product characterization. Chemical reaction engineering consists of analysis of the factors governing the process in order to establish the reactor equations. The factors are geometric, hydrodynamic, physical and physicochemical.[9] While the first factor consists of the description of the geometry of the reactor, the second is the hydrodynamic factor dealing with the flow of each phase and with the way those phases are put into contact and mixed. The hydrodynamic factor is also closely linked with the physical factor relating the phenomena of transport and transfer of mass, heat and momentum quantity.[10] Finally, the last factor consists of physicochemical factors, in relation to thermodynamic data and the kinetics of the reaction. These four factors allow the linking of the results of the reaction to the operating variables, and a knowledge of relationships between all the operating factors is necessary in order to establish the equations of the reactor. In this article, each factor is studied in order to simulate the reactor performance.

Experiments

Catalyst and reaction gases

The catalyst used for this study is a bimetallic catalyst supported on alumina, synthesized according to a method similar to that described by Tran et al.[11]

During the reaction, ethylene is used as the carbon source, balanced by nitrogen as the inert gas and/or by hydrogen, and is decomposed on the surface of the catalyst into solid carbon and gaseous hydrogen.

Experimental setup

The discontinuous experimental setup for kinetic measurements consists of a discontinuous tubular reactor used to determine the carbon nanotube synthesis reaction rate by using a mass spectrometer, which allows the reaction rate to be inferred from exhaust gas composition measurements.[12,13] The use of the mass spectrometer enables the determination of both the initial reaction rate as a function of temperature and hydrocarbon partial pressure, and catalytic deactivation law. Indeed, the initial reaction rate corresponds to the maximum reaction rate, which decreases as a function of time resulting from the formation of amorphous carbon. The continuous reactor is schematically described in Figure 1. The reactor consists of a tubular inclined rotary kiln with a mobile bed, equipped with continuous systems for catalyst feeding and for the collection of gaseous and solid products, of a mass spectrometer for analyzing the output gas composition, and of a completely automated system of control and acquisition of data. The operating conditions consist of the continuous feeding of gas and solid catalyst under inert atmosphere, and in the continuous collection of reaction products under inert atmosphere. So, contact between hydrocarbon and oxygen from the air is avoided. Material flow is made possible by the gravity force resulting from the rotation and inclination of the reactor. The rotation speed and the inclination angle allow the determination of the solid material residence time. The system assures mechanical resistance and rotating

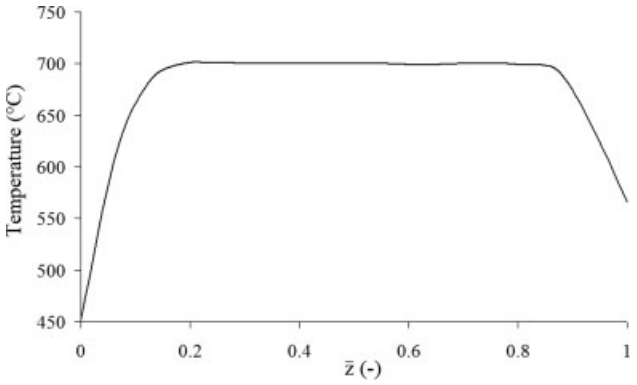

Figure 2. Reactor temperature profile at 700°C.

tightness between the mobile part and the fixed part of the reactor, for temperatures of up to 1,050°C.[8]

Experimental design

While experimental measurements corresponding to the discontinuous reactor have been previously published,[12,13] the experimental design performed in this study and corresponding to continuous reactor measurements consists of a feed gas composed of ethylene, nitrogen and hydrogen. The operating pressure and temperature are, respectively, equal to 1 atm and 700°C, because it has been previously determined that 700°C corresponds to the temperature leading to the best productivity.[12] It has to be noted that the reaction temperature is limited to 700°C, since at higher temperatures, homogeneous phase decomposition of ethylene occurs and soot is formed. The reactor temperature profile at 700°C is presented on Figure 2. Reactor rotation speed varies from 0.5 to 5 rpm, while the inclination angle ranges between 0.5 and 5°. For each rotation speed linked to an inclination angle, the corresponding residence time is determined by measuring the average time needed by the product to flow to the reactor exit.

Modeling

Geometric and hydrodynamic factors

The reactor used in this study is a continuous tubular rotary kiln. This technology allows a continuous feeding of the solid catalyst and of the input gas (C_2H_4, balanced by N_2 and/or H_2), and the continuous collection of the produced solid and of the output gas. Both reaction gas and catalyst are introduced into the entry side of the reactor, allowing cocurrent flows of gas and solid inside the reactor.

The Reynolds number *Re* allows to determine the flow regime. The Reynolds number *Re* quantifies the ratio between inertial forces and viscous forces.[14]

$$Re = \frac{u\, d_r}{v} \tag{1}$$

where u is the total gas velocity, d_r is the diameter of the reactor, and v is the kinematic viscosity of the gas. The total gas velocity u can be calculated by

$$u = \frac{F\, V_M}{\frac{\pi\, d_r^2}{4}} \tag{2}$$

The kinematic viscosity of a gas is the ratio between the dynamic viscosity μ and the density ρ_g of the gas[15]

$$v = \frac{\mu}{\rho_g} \tag{3}$$

The dynamic viscosity μ is based on the potential of energy of Lennard-Jones[15]

$$\mu = 2.6693 \times 10^{-6} \frac{\sqrt{MT}}{\sigma^2 \Omega_\mu} \tag{4}$$

where T, M, σ and Ω_μ are, respectively, the temperature, the molecular mass, the collision diameter and the collision integral. The dynamic viscosity is, respectively, equal to 2.65×10^{-5} Pa.s, 2×10^{-5} Pa.s and 4.08×10^{-5} Pa.s for ethylene, hydrogen and nitrogen at 700°C.

For a gas phase composed of several gases, the dynamic velocity is estimated by[15]

$$\mu = \sum_{i=1}^{n} \frac{x_i \mu_i}{\sum_j x_j \Phi_{ij}} \tag{5}$$

where x_i and x_j represent the molar fraction of composant i and j, and Φ_{ij} is given by[15]

$$\Phi_{ij} = \frac{1}{\sqrt{8}} \left(1 + \frac{M_i}{M_j}\right)^{-\frac{1}{2}} \left[1 + \left(\frac{\mu_i}{\mu_j}\right)^{\frac{1}{2}} \left(\frac{M_j}{M_i}\right)^{\frac{1}{4}}\right]^2 \tag{6}$$

where M_i and M_j represent the molecular mass of composant i and j.

For the experimental conditions studied in this research, the Reynolds number *Re* varies from 100 to 600. So the gas flow in the reactor is a laminar flow, because it is smaller than 2,100.[15]

The reactor modeling is based on the plug-flow approximation, for both gas and solid. In order to prove that the plug-flow hypothesis is correct, the dimensionless Peclet number *Pe* has to be estimated. The Peclet number *Pe* quantifies the ratio between the rate of advection of a flow to its rate of diffusion.[16] The higher the Peclet number *Pe*, the more the flow tends to be a plug flow. Villermaux considers that the plug-flow approximation is definitely verified for a value of the Peclet number *Pe* of higher than 100.[9]

For the solid phase and for experimental conditions considered in this article, carbon nanotubes flow in the slumping mode or in the rolling mode, depending on the rotational speed and on the filling percentage of the reactor.[17] In these conditions, the Peclet number *Pe* for the solid phase is of the order of 10^2–10^4,[18] and the solid flow can be considered as a plug-flow.

The Peclet number *Pe* for the gas is defined by[16]

$$Pe = \frac{u\, L}{D_L} \tag{7}$$

where u is the total gas velocity, L is the useful length of the reactor, and D_L is the axial diffusivity of ethylene.

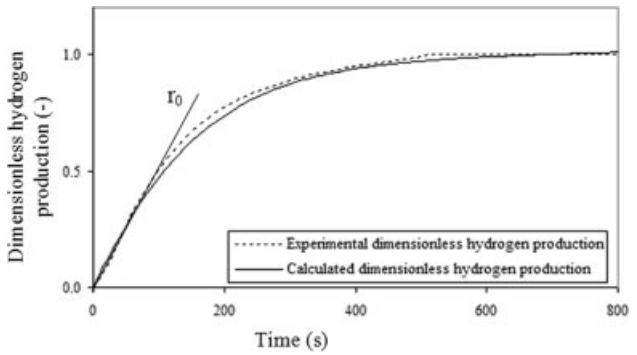

Figure 3. Comparison between experimental and calculated dimensionless hydrogen production curves for a feed gas composed of 90% C_2H_4 and 10% H_2 at 700°C.

The axial diffusivity of ethylene is the sum of two contributions[9]

$$D_L = D_m + \frac{u^2 d_r^2}{192 D_m} \tag{8}$$

where D_m is the molecular diffusivity of ethylene, which is equal to 4.5×10^{-4} $m^2.s^{-1}$ in hydrogen at 700°C.[12]

For the experimental conditions studied in this research, the Peclet number Pe varies from 10 to 40, with back mixing being more important in this study. However, the ethylene conversion in the reactor is rather weak and never exceeds 50%. For an ethylene conversion equal to 50% and for a Peclet number Pe equal to 10, the reactor can be compared to a tanks-in-series reactor with more than 5 tanks in series.[14] In this case, the error in the performance of the reactor is below 7%. It can be concluded that the plug-flow hypothesis can be considered to be valid.

Physicochemical factor

This factor deals with the initial reaction rate and the catalytic deactivation during the reaction. The design and the development of an industrial reactor require the determination of the apparent reaction rate as a function of catalyst, temperature, total gas flow rate and partial pressure. The initial true reaction rate with external catalytic bed surface conditions as a function of partial pressure and temperature has been previously determined.[12] The general equation can be written as follows

$$r_0 = \frac{A \exp\left(-\frac{(E_a + \Delta H^\circ)}{RT}\right) P_{C_2H_4}}{1 + \exp\left(-\frac{\Delta H^\circ}{RT}\right) \exp\left(\frac{\Delta S^\circ}{R}\right) P_{C_2H_4}} \tag{9}$$

where E_a is the activation energy, ΔH° is the ethylene standard adsorption enthalpy, and ΔS° is the standard ethylene adsorption entropy. The parametric adjustment on data obtained at 700°C leads to the kinetic equation

$$r_0 = \frac{0.0034 P_{C_2H_4}}{1 + 0.62 P_{C_2H_4}} \left(kmol_{C2H4}.kg_{catalyst}^{-1}.s^{-1}\right) \tag{10}$$

As shown in Figure 3, the initial reaction rate corresponds to the maximum reaction rate and remains constant for a period of only 100 s. After that time, the reaction rate decreases and becomes progressively equal to zero. The cause of the decrease in reaction rate is catalytic deactivation due to the formation of amorphous carbon. Indeed, such a formation does not allow the hydrocarbon to reach active sites covered by amorphous carbon.[19] So, catalytic deactivation has to be taken into account in order to model carbon nanotube production in the rotary kiln.

Several empirical deactivation models have been tested on data previously used to determine initial reaction rate.[12] The best model corresponds to a sigmoid catalytic deactivation. Parametric equations corresponding to this model are written as follows

$$r = \overline{m} r_0 \tag{11}$$

$$\frac{d[H_2]}{dt} = 2r \tag{12}$$

$$\frac{d\overline{m}}{dt} = \frac{-b}{\cosh^2(d(t-a))} \tag{13}$$

where r_0, r and $\overline{m}$ are, respectively, the initial specific reaction rate, the specific reaction rate and the dimensionless active mass of catalyst. It has to be noted that this deactivation model corresponds to the best deactivation law for all the other tested catalysts.

Estimates allow the determination of parameters a, b and d for each experimental condition. Figure 3 shows good agreement between the experimental hydrogen production curve and the hydrogen production curve resulting from the sigmoid deactivation model. In Figure 3, the dimensionless hydrogen production is highlighted, reported to the total hydrogen production reached at the end of the reaction. The corresponding catalytic deactivation law is presented in Figure 4.

Parameters a, b and d have been adjusted as a function of the operating conditions. Adjustment results indicate that a is equal to zero, whatever the operating conditions, while b and d are linear decreasing functions of the hydrogen partial pressure, as shown in Figure 5. It means that hydrogen, respec-

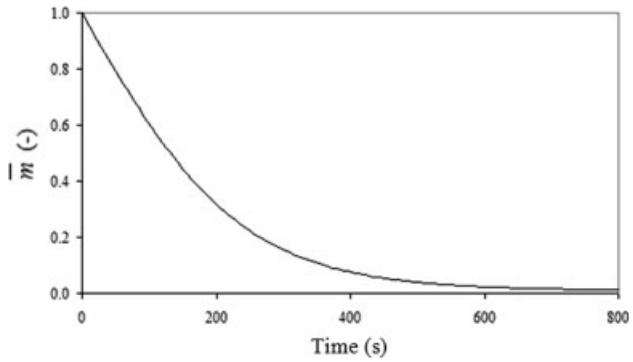

Figure 4. Relative mass of active catalyst for a feed gas composed of 90% C_2H_4 and 10% H_2 at 700°C.

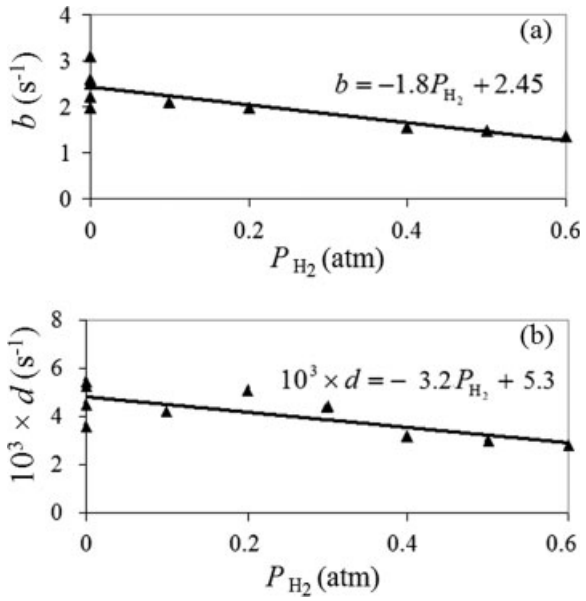

Figure 5. Dependence of (a) parameter *b*, and (b) parameter *d* as a function of the hydrogen pressure.

tively, slows down and delays the catalytic deactivation. This result can be explained by the role of hydrogen on amorphous carbon production. Indeed, hydrogen reduces the rate of carbon production by dehydrogenation so that carbon nanotubes can be produced rather than less thermodynamically stable soot and carbon fibers.[20]

Physical factor

This factor deals with mass and heat transport in the reactor. The physical limitation leading to the decrease in the reaction rate may stem from a vertical concentration gradient within the catalytic bed. When molecules of ethylene reach the surface of the catalytic bed, they have to diffuse through the catalytic bed before reacting. If diffusion of ethylene occurs much more easily than the chemical reaction, then the concentration gradient within the catalytic bed will be negligible. On the other hand, if diffusion is the limiting factor, a given molecule of ethylene would have many opportunities to react before penetrating deeply into the catalytic bed. In such a case, only the superficial layer of the catalytic bed would actually be active in the reaction. The Thiele dimensionless number φ_s is used to quantify this physical limit. The square of the Thiele modulus, is, therefore, interpreted as the ratio of the specific reaction rate calculated at the external catalytic bed surface, to the diffuse flow of ethylene per unit of surface of the catalytic bed[9,14,16,21]

$$\varphi_s = \sqrt{\frac{r_s \rho d_b^2}{D_e C_s}} \tag{14}$$

where r_s is the specific reaction rate with external catalytic bed surface conditions, d_b is the thickness of the catalytic bed, ρ is the specific mass of catalytic bed, D_e is the effective diffusivity of ethylene,[12] and C_s is the ethylene concentration at the external catalytic bed surface. While C_s is calculated by dividing ethylene partial pressure $P_{C_2H_4}$ by the temperature T equal to 973 K, and by the gas constant R, ρ is obtained by measuring the mass of a given volume of catalyst, and is equal to 1.05×10^3 kg.m^{-3}. The reaction rate r_s is determined by using Eq. 10 for the ethylene partial pressure reaction. The effective diffusivity of ethylene D_e takes the tortuosity factor of catalyst τ_p, and the void fraction of catalytic bed ε into account, according to the relationship

$$D_e = \frac{D_m \varepsilon}{\tau_p} \tag{15}$$

If $\varphi_s < 1$, the ethylene molar fraction is almost a constant over the whole thickness of the catalytic bed. If $\varphi_s > 1$, a steep gradient develops near its surface and only a fraction of the catalytic bed is active.

The effectiveness factor η_s[9,14,16,21] is defined as the ratio of the apparent reaction rate r_a to the reaction rate r_s, which would be observed if diffusion was not a limiting factor.

For a first-order reaction, the effectiveness factor η_s is found to be equal to

$$\eta_s = \frac{\tanh(\varphi_s)}{\varphi_s} \tag{16}$$

This function is almost equal to 1 for $\varphi_s < 1$, and decreases as $1/\varphi_s$ for larger values of Thiele modulus ($\varphi_s > 1$).

For a zero-order reaction, the effectiveness factor η_s is equal to 1, whatever the value of the Thiele modulus. Indeed, a zero-order reaction does not depend on the concentration profile inside the catalytic bed.

If the hypothesis is made that only a quarter of the reactor circumference is covered by catalyst (a conservative hypothesis), the thickness d_b of the catalytic bed is estimated by

$$d_b = \frac{\dot{m}_s / u_s \rho}{\pi d_r / 4} \tag{17}$$

where $\dot{m}_s$ is the catalyst flow rate, ρ is the specific mass of the catalytic bed, and d_r the reactor diameter.

The worst experimental conditions with regard to the depth of the catalytic bed performed in this study correspond to the highest catalyst flow rate, and to the longest residence time in the reactor. In such experimental conditions, d_b is smaller than 0.3×10^{-3} m. Once the thickness of the catalytic bed d_b is known, the Thiele modulus φ_s can be calculated by considering an average tortuosity factor τ_p, and a void fraction of the catalytic bed ε equal to 3.5 and 0.45, respectively.[16] Furthermore, r_s is obtained by using Eq. 10, with the reaction ethylene partial pressure $P_{C_2H_4}$. The Thiele modulus φ_s for the first-order reaction is found to be smaller than 0.6 whatever the ethylene concentration in the feed gas. The corresponding effectiveness factor η_s is equal to 0.89. It also has to be noted that residence times are very long, which does not correspond to conditions applied for industrial production. In practice, the residence times are smaller than 1,800 s, and the ethylene partial pressure is around 0.7 atm, corresponding to a Thiele modulus φ_s of smaller than 0.165,

and to an effectiveness factor of greater than 0.985. While the previous calculated effectiveness factor corresponds to a first-order reaction, a zero-order reaction gives a factor equal to 1. At 700°C, the experimental reaction gives a factor equal to 0.79.[12] So the corresponding effectiveness factor varies between 0.985 and 1. Furthermore, the rolling of the particles on the catalytic bed was not taken into account in calculating the Thiele modulus φ_s. Indeed, the rolling movement increases mass-transfer phenomena between gas and solid. It can be concluded that diffusion of ethylene occurs much more quickly than the chemical reaction, and that ethylene diffusion though the catalytic bed is not the kinetic limiting factor.

Reactor equations

Once the four factors governing the reactor are known, the modeling of the continuous inclined rotary kiln is made possible on the basis of a co-current plug-flow model for gas and solid. The general equation of hydrocarbon decomposition into solid carbon nanotubes and gaseous hydrogen is $C_mH_n \rightarrow m\,C + \frac{n}{2}\,H_2$. The mass balances are written as follows

- For the solid flow:

$$\frac{d\dot{m}_c}{dz} = v_C M_C r \frac{\dot{m}_s}{u_s} \tag{18}$$

- For the total gas flow:

$$\frac{dF}{dz} = (v_{H_2} + v_{C_mH_n}) r \frac{\dot{m}_s}{u_s} \tag{19}$$

- For the hydrocarbon flow:

$$\frac{dF_{C_mH_n}}{dz} = v_{C_mH_n} r \frac{\dot{m}_s}{u_s} \tag{20}$$

Several dimensionless variables can be defined

$$\overline{z} = \frac{z}{L} \tag{21}$$

$$\overline{r} = \frac{r}{r_m} \tag{22}$$

where r_m is the maximum reaction rate that can be reached experimentally, corresponding to a hydrocarbon partial pressure of 1 atm

$$\tau = \frac{M_C r_m L}{u_s} \tag{23}$$

$$\overline{\dot{m}}_C = \frac{\dot{m}_c}{\dot{m}_s} \tag{24}$$

with $\overline{\dot{m}}_C$ corresponding to the specific productivity of carbon nanotubes

$$\overline{F} = \frac{M_C F}{\dot{m}_s} \tag{25}$$

$$\overline{F}_{C_mH_n} = \frac{M_C F_{C_mH_n}}{\dot{m}_s} \tag{26}$$

So with dimensionless variables, mass balances become:

- For the solid flow:

$$\frac{d\overline{\dot{m}}_C}{d\overline{z}} = v_C \tau \overline{r} \tag{27}$$

- For the total gas flow:

$$\frac{d\overline{F}}{d\overline{z}} = (v_{H_2} + v_{C_mH_n}) \tau \overline{r} \tag{28}$$

- For the hydrocarbon flow:

$$\frac{d\overline{F}_{C_mH_n}}{d\overline{z}} = v_{C_mH_n} \tau \overline{r} \tag{29}$$

In this case of ethylene decomposition into solid carbon nanotubes and gaseous hydrogen, the general hydrocarbon decomposition equation is written $C_2H_4 \rightarrow 2C + 2H_2$. Then in Eqs. 27 to 29, $v_C = 2$, $v_{C_mH_n} = -1$ and $v_{H_2} = 2$, while in Eq. 22, r_m can be formulated more precisely

$$r_m = r(P_{C_2H_4} = 1\text{atm}) = \frac{0.0034}{1.62} = 2.1 \times 10^{-3}\ \text{kmol}_{C_2H_4}.\text{s}^{-1}.\text{kg}_{\text{catalyst}}^{-1} \tag{31}$$

Furthermore, due to catalyst deactivation, a deactivation equation has to be taken into account. Reaction rate expression can then be deduced from Eq. 10

$$r = \overline{m} \frac{0.0034 P_{C_2H_4}}{1 + 0.62 P_{C_2H_4}} \tag{31}$$

where $\overline{m}$ is the dimensionless active mass of catalyst.

In order to describe the evolution of $\overline{m}$ through the reactor, Eq. 13, which is written as a function of time, must be considered. The deactivation equation is obtained by modifying Eq. 13 as a function of the longitudinal variable in the reactor z, according to the relationship $z = u_s t$

$$\frac{d\overline{m}}{dz} = \frac{-b}{u_s \cosh^2(d(\frac{z}{u_s} - a))} \tag{32}$$

where u_s corresponds to the average solid flow rate through the reactor. u_s is calculated by dividing the length of the useful part of the rotating reactor L, by the residence time.

Three dimensionless parameters of catalytic deactivation can be defined

$$\overline{a} = \frac{a u_s}{L} \tag{33}$$

$$\overline{b} = \frac{bL}{u_s} \tag{34}$$

$$\overline{d} = \frac{dL}{u_s} \tag{35}$$

So the catalytic deactivation equation becomes

$$\frac{d\overline{m}}{d\overline{z}} = \frac{-\overline{b}}{\cosh^2\left(\overline{d}(\overline{z} - \overline{a})\right)} \tag{36}$$

The four continuous reactor dimensionless equations corresponding to ethylene decomposition are

$$\frac{d\overline{\dot{m}}_C}{d\overline{z}} = 2\tau\overline{r} \tag{37}$$

$$\frac{d\overline{F}}{d\overline{z}} = \tau\overline{r} \tag{38}$$

$$\frac{d\overline{F}_{C_2H_4}}{d\overline{z}} = -\tau\overline{r} \tag{39}$$

$$\frac{d\overline{m}}{d\overline{z}} = \frac{-\overline{b}}{\cosh^2\left(\overline{d}(\overline{z}-\overline{a})\right)}$$

Discussion

The system of four differential equations can be solved for each set of experimental conditions, by applying the initial conditions at the reactor inlet that correspond to the initial dimensionless total gas flow rate $\overline{F}$, the initial dimensionless ethylene flow rate $\overline{F}_{C_2H_4}$, the initial dimensionless carbon flow rate $\overline{\dot{m}}_C$ (always equal to zero), and the initial dimensionless active mass of catalyst $\overline{m}$ (always equal to one). The resolution of differential equations allows us to obtain the evolution of partial pressure, of the dimensionless carbon flow rate $\overline{\dot{m}}_C$, that is, the carbon productivity, and of the dimensionless active mass of the catalyst through the reactor $\overline{m}$, for a given set of experimental conditions. The discussion is divided into two different parts. The first part consists of studying the variation of the carbon nanotube specific productivity $\overline{\dot{m}}_C$ through the reactor, related to several operating variables such as dimensionless residence time of solid τ, initial dimensionless total gas flow rate $\overline{F}$, and initial dimensionless ethylene total gas flow rate $\overline{F}_{C_2H_4}$. The second part of the discussion consists of a comparison of results obtained from equation modeling and those from the experiments.

First, the systems of differential equations were solved for two different sets of initial conditions, with a feed gas composition of 60% ethylene, 20% hydrogen and 20% nitrogen. The two sets of initial conditions differ by the dimensionless total gas flow rate $\overline{F} = \frac{M_C F}{\dot{m}_s}$, quantifying the ratio between the total gas flow rate F, and the catalyst flow rate $\dot{m}_s$. $\overline{F}$ is, respectively, equal to 32.12, corresponding to a set of experimental conditions tested in this study, and to 10.71, with values three times smaller than the previous one. So if $\dot{m}_s$ is the same for the two sets of initial conditions, F is three times greater for the first set of initial conditions than for the second one. This means that for the first set of initial conditions, the catalyst is in contact with a greater amount of reaction gas. The curves corresponding to each of those initial experimental conditions for the four different dimensionless residence times are represented in Figures 6 and 7, respectively, as a function of the dimensionless longitudinal variable in the reactor $\overline{z}$. Several conclusions can be drawn.

- For each set of initial conditions, the greater the residence time, the greater the specific productivity $\overline{\dot{m}}_C$, the catalytic deactivation, and the hydrocarbon consumption.
- For very small residence times, the ethylene partial pressure does not decrease significantly, and the productivity is weak.

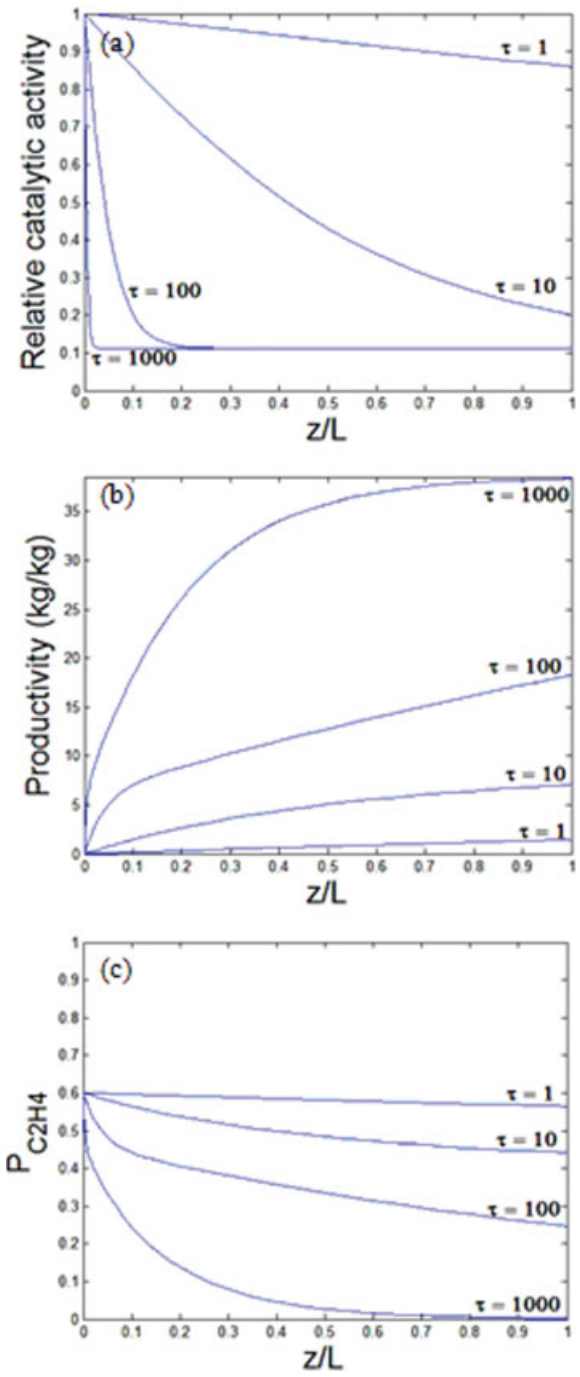

Figure 6. Evolution (a) of relative catalytic activity, (b) of productivity of carbon, and (c) of ethylene partial pressure for $\overline{F}$ = 32.12, $\overline{F}_{C_2H_4}$ = 19.27, $\overline{\dot{m}}_C$ = 0 and $\overline{m}$ = 1 at $\overline{z}$ = 0.

[Color figure can be viewed in the online issue, which is available at www.interscience.wiley.com.]

- On the other hand, for longer residence times, the ethylene consumption and the productivity are more important. Due to catalytic deactivation, very long residence times (τ greater than 1,000) are necessary in order to reach maximum productivity. Maximum productivity also depends on the initial experimental conditions. Indeed, the number of deposed

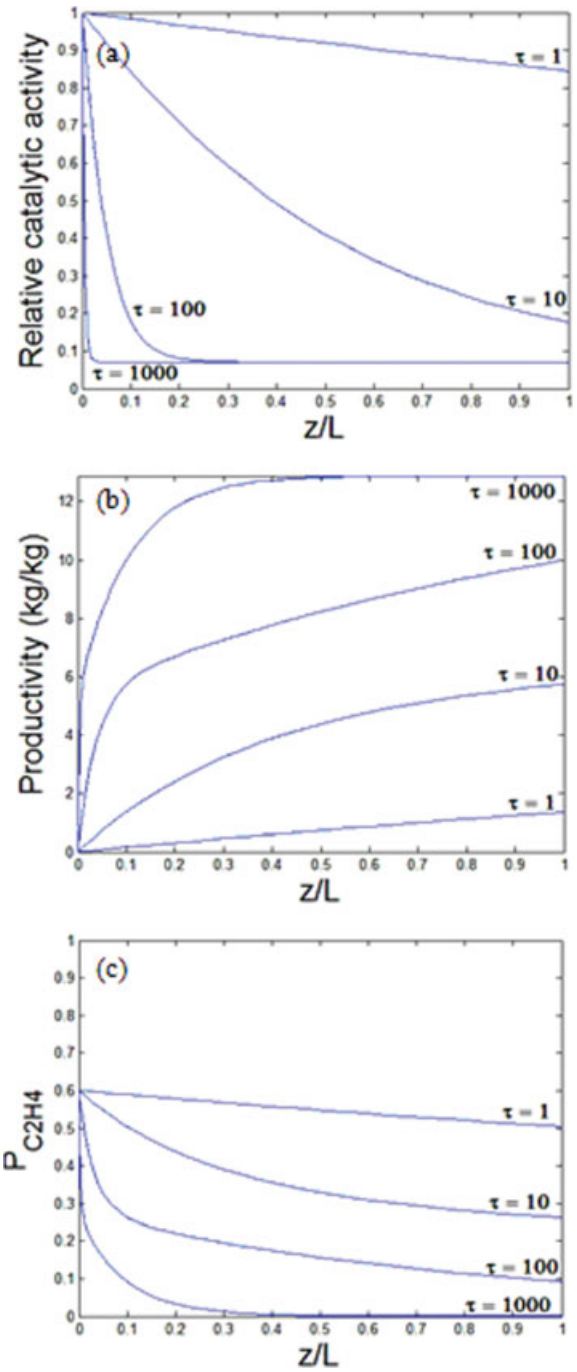

Figure 7. Evolution (a) of relative catalytic activity, (b) of productivity of carbon, and (c) of ethylene partial pressure for $\overline{F} = 10.71, \overline{F}_{C_2H_4} = 6.44$, $\overline{\dot{m}}_C = 0$ and $\overline{m} = 1$ at $\overline{z} = 0$.

[Color figure can be viewed in the online issue, which is available at www.interscience.wiley.com.]

carbon atoms cannot be greater than the number of carbon atoms introduced into the reactor. So the maximum productivity $\overline{\dot{m}}_C$ is twice the dimensionless ethylene flow rate $\overline{F}_{C_2H_4}$. Therefore, if a given productivity is required ($\overline{\dot{m}}_C$ equal to 40 for example), the ethylene flow rate must be controlled accordingly ($\overline{F}_{C_2H_4}$ equal or greater than 20 for the same example). It can be added that the dimensionless residence time τ has to be chosen in order that the whole length of the reactor is used. Indeed, if the residence time is too long, the catalyst will deactivate, ethylene partial pressure will no longer decrease, and productivity will not increase significantly. For example, in Figure 6b and for $\tau = 10$, half of the maximum carbon production is reached in the first third of the reactor length. In the last section of the reactor, the relative catalytic activity and the production of carbon nanotubes are very weak, while ethylene partial pressure does not decrease significantly. In this case, shorter residence times would be considered to obtain similar productivity at the reactor outlet without extra time.

The influence of total gas flow rate F for a given gas composition, and for a given catalytic flow rate $\dot{m}_s$ is highlighted by the comparison between Figures 6 and 7. The ethylene partial pressure $P_{C_2H_4}$ decreases more rapidly for a small total gas flow rate, as shown in Figure 7c, corresponding to a dimensionless total gas flow rate $\overline{F}$, three times smaller than in Figure 6c. Indeed, a smaller amount of carbon is introduced into the reactor with the same catalytic flow rate $\dot{m}_s$. So a greater percentage of ethylene is decomposed in solid

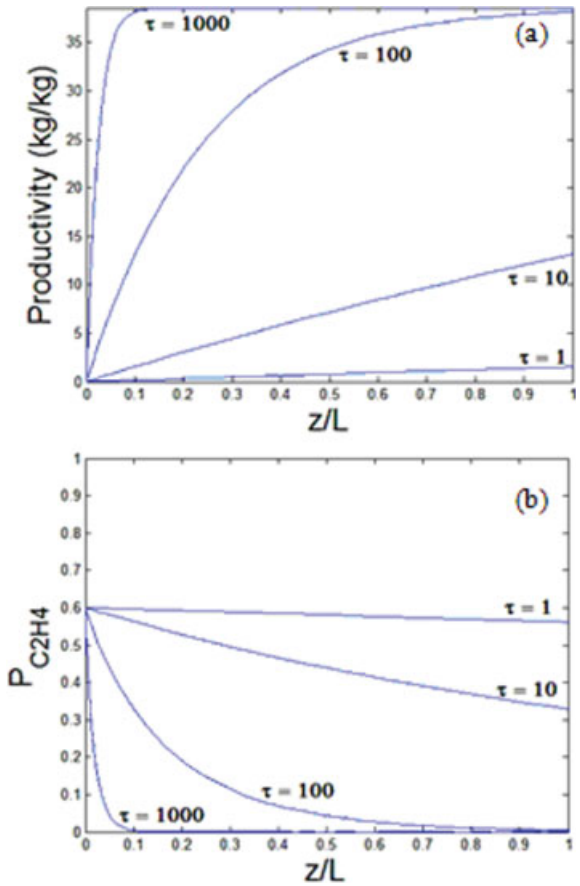

Figure 8. Profiles of (a) carbon productivity, and (b) ethylene partial pressure for $\overline{F} = 32.12, \overline{F}_{C_2H_4} = 19.27$, $\overline{\dot{m}}_C = 0$ at $\overline{z} = 0$, and without deactivation.

[Color figure can be viewed in the online issue, which is available at www.interscience.wiley.com.]

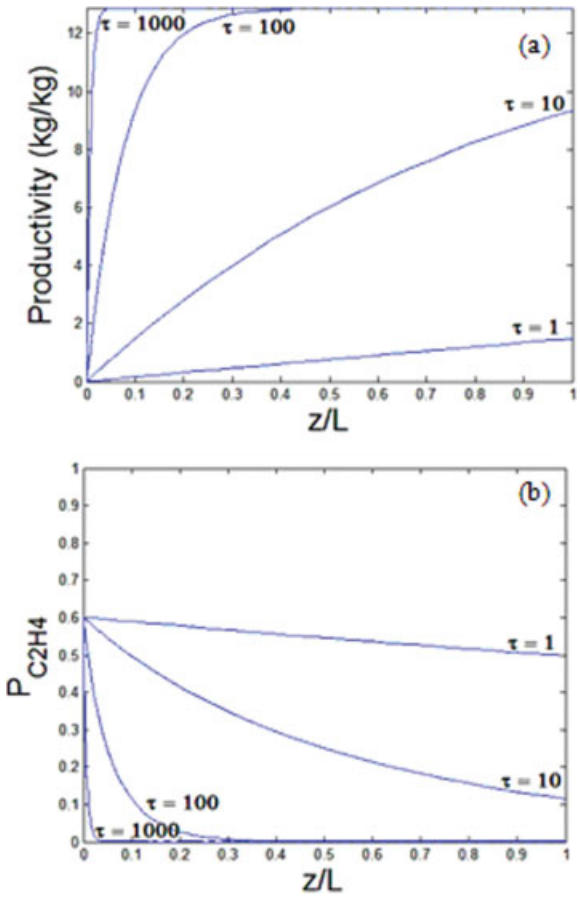

Figure 9. Profiles of (a) carbon productivity and (b) ethylene partial pressure for $\overline{F}$ = 10.71, $\overline{F}_{C_2H_4}$ = 6.44, $\overline{m}_C$ = 0 at $\overline{z}$ = 0, and without deactivation.

[Color figure can be viewed in the online issue, which is available at www.interscience.wiley.com.]

carbon. As for the catalytic deactivation (Figures 6a and 7a), this does not change significantly, while the specific productivity $\overline{m}_C$ reaches maximum productivity corresponding to two times the ethylene gas flow rate $\overline{F}_{C_2H_4}$, more rapidly through the reactor and for smaller dimensionless residence time τ (Figures 6a and 7a). This can be explained by the fact that the deactivation curves are not very different. So the catalytic activity becomes less through the reactor, whatever the amount of ethylene introduced in the reactor, avoiding the decomposition of a great amount of ethylene. In other words, the catalyst with a given activity is able to decompose a certain number of ethylene molecules, while the excess of ethylene cannot be decomposed.

The system of differential equations was also solved without taking catalytic deactivation into account. This is the ideal situation that further development of catalysts should reach. In this case, the relative catalytic activity m is equal to 1 all through the reactor. Figures 8 and 9 represent the productivity and the ethylene partial pressure profiles for the same two sets of initial experimental conditions. The maximum productivity corresponding to a given set of initial conditions is reached faster than with catalytic deactivation for given shorter residence times. So without catalytic deactivation, shorter residence times are needed to obtain the maximum productivity. Concerning the influence of dimensionless total gas flow rate $\overline{F}$, it can be observed that for the smaller dimensionless total gas flow rate $\overline{F}$, the maximum specific productivity is reached more rapidly along the reactor, for a given dimensionless residence time τ (Figure 8a and b). However, the maximum specific productivity that can be reached, twice the ethylene gas flow rate $\overline{F}_{C_2H_4}$, is smaller.

The influence of hydrogen partial pressure on catalytic deactivation and on carbon specific production was also studied. The specific productivity obtained with a feed gas composed of ethylene and hydrogen only is a little higher than the specific production obtained with ethylene balanced by helium only (Figure 10a). The reason for this is that catalytic deactivation depends on hydrogen partial pressure (Figure 5). Indeed, the presence of hydrogen delays catalytic deactivation (Figure 10b), while hydrogen does not influence the reaction rate, which depends only on ethylene partial pressure (Eq. 10).

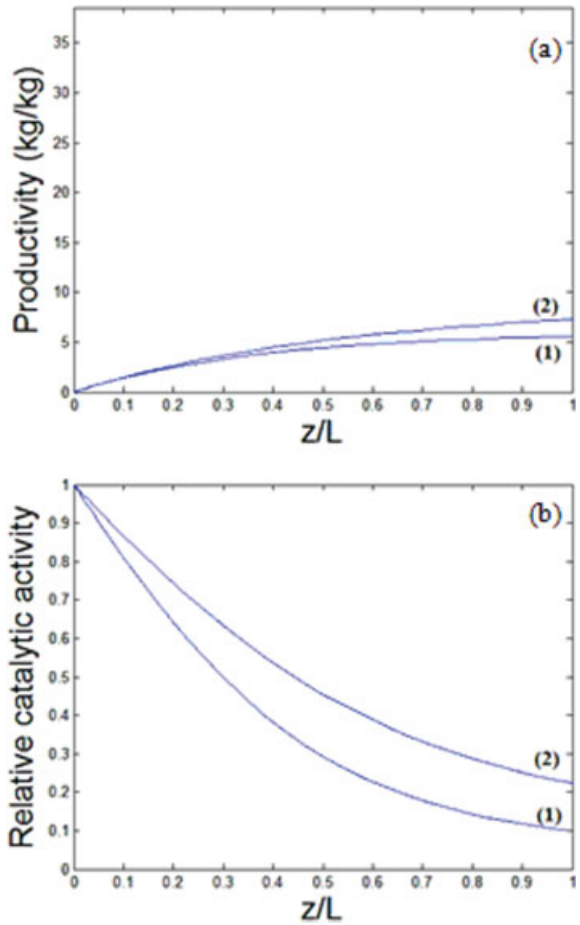

Figure 10. Profiles of (a) carbon productivity, and (b) relative catalytic activity for $\overline{F}$ = 32.12, $\overline{F}_{C_2H_4}$ = 19.27, (1) without hydrogen, or (2) with hydrogen $\overline{m}_C$ = 0 and $\overline{m}$ = 1 at $\overline{z}$ = 0.

[Color figure can be viewed in the online issue, which is available at www.interscience.wiley.com.]

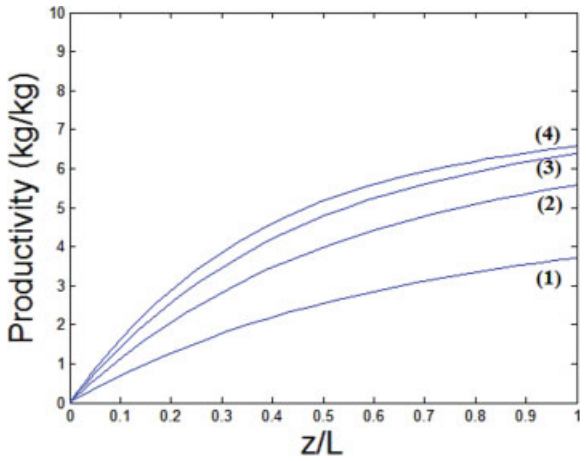

Figure 11. Profiles of specific productivity for $\overline{F}$ = 32.12, (1) $\overline{F}_{C_2H_4}$ = 6.425, (2) $\overline{F}_{C_2H_4}$ = 12.85, (3) $\overline{F}_{C_2H_4}$ = 19.27, and (4) $\overline{F}_{C_2H_4}$ = 25.7, $\dot{\overline{m}}_C$ = 0 and $\overline{m}$ = 1 at $\overline{z}$ = 0, and for τ = 10, and with catalyst deactivation.

[Color figure can be viewed in the online issue, which is available at www.interscience.wiley.com.]

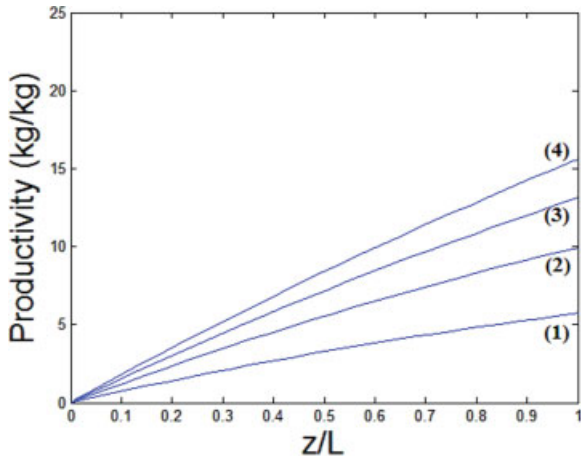

Figure 12. Profiles of specific productivity for $\overline{F}$ = 32.12, (1) $\overline{F}_{C_2H_4}$ = 6.425, (2) $\overline{F}_{C_2H_4}$ = 12.85, (3) $\overline{F}_{C_2H_4}$ = 19.27, and (4) $\overline{F}_{C_2H_4}$ = 25.7 and $\dot{\overline{m}}_C$ = 0 at $\overline{z}$ = 0, for τ = 10, and without catalytic deactivation.

[Color figure can be viewed in the online issue, which is available at www.interscience.wiley.com.]

Finally, the influence of gas composition for a given total gas flow rate and nitrogen flow rate was also studied. Results are presented in Figures 11 and 12, respectively, with and without catalytic deactivation. Conclusions show that the greater the amount of ethylene introduced into the reactor, the greater the specific productivity. However, catalytic deactivation increases with the ethylene flow rate in the feed gas, leading to a decrease in carbon specific productivity relative to the introduced carbon. The reason for this is that lower hydrogen partial pressure increases catalytic deactivation.

Table 1. Experimental Design

τ (-)	$\overline{F}_{C_2H_4}$ ($kg_{carbon}.kg^{-1}_{catalyst}$)	$\overline{F}_{H_2}$ ($kg_{carbon}.kg^{-1}_{catalyst}$)	$\overline{F}_{N_2}$ ($kg_{carbon}.kg^{-1}_{catalyst}$)	$\overline{F}$ ($kg_{carbon}.kg^{-1}_{catalyst}$)	$\dot{\overline{m}}_C$ ($kg_{carbon}.kg^{-1}_{catalyst}$)
4.3	19.27	6.42	6.42	32.12	6.7
5.2	32.12	32.12	32.12	32.12	8.4
					6.9
8.6	28.91	12.85	6.42	48.18	7.9
	19.27	6.42	6.42	32.12	9.3
	9.64	0.00	6.42	16.06	6.5
25.0	19.27	6.42	6.42	32.12	8.0
					7.7
					8.4
25.8	28.91	12.85	6.42	48.18	9.8
	19.27	6.42	6.42	32.12	9.6
					10.2
					9.6
					9.7
					9.8
	9.64	0.00	6.42	16.06	7.3
35.3	19.27	6.42	6.42	32.12	9.4
					9.2
43.0	28.91	12.85	6.42	48.18	8.8
	19.27	6.42	6.42	32.12	9.3
	9.64	0.00	6.42	16.06	7.6
51.7	19.27	6.42	6.42	32.12	6.8
19.8	30.51	6.42	6.42	43.36	12.7
	19.27	6.42	6.42	42.84	13.6
	6.42	6.42	6.42	25.70	6.9
25.8	30.51	6.42	6.42	57.83	12.7
	19.27	6.42	6.42	42.84	9.7
	6.42	6.42	6.42	25.70	6.4
31.9	30.51	6.42	6.42	57.83	9.6
	19.27	6.42	6.42	42.84	10.5
	6.42	6.42	6.42	25.70	6.1

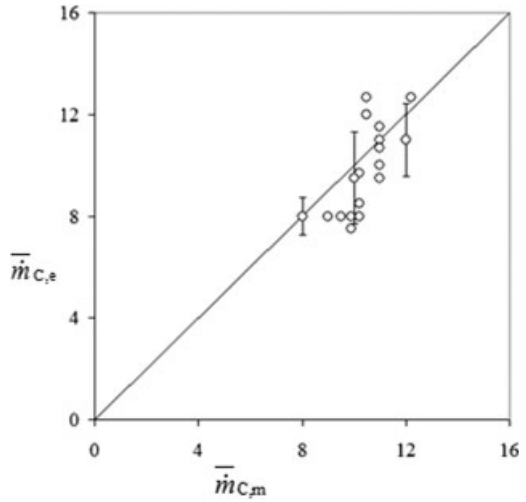

Figure 13. Comparison between experimental and calculated production.

Without catalytic deactivation, the specific productivity depends only on the ethylene flow rate in the feed gas $\overline{F}_{C_2H_4}$. Dimensionless residence time τ equal to 10 is too small to reach a maximum specific productivity equal to twice the dimensionless ethylene flow rate $\overline{F}_{C_2H_4}$.

In a second step, results obtained from equation modeling were compared with experimental results. The experimental design and dimensionless carbon nanotube flow rate data relating to the operating conditions are presented in Table 1. Figure 13 represents the comparison between experimental dimensionless carbon nanotube flow rate $\overline{\dot{m}}_{C,e}$ and dimensionless carbon nanotube flow rate calculated using the model rate $\overline{\dot{m}}_{C,m}$, and this shows a very good agreement between calculated and experimental flow rate. This result shows that the hypotheses chosen in order to establish the model are valid. First of all, the plug-flow model applied to solid and gas flows in the reactor is valid, although the Peclet number *Pe* for the gas flow is a little smaller than 100, the limit above which the plug-flow hypothesis is considered to be definitively valid. This is all the more correct because the conversion rate of ethylene is weak. Second, the effectiveness factor of the catalytic bed η_s is equal to 1. Consequently, the physical factors, that is, phenomena of mass transport and mass transfer toward and through the catalytic bed, can be neglected. As a conclusion, the apparent kinetic of the reaction in the reactor is the true kinetic, taking catalytic deactivation into account.

Conclusions

According to chemical reaction engineering, the four factors governing carbon nanotube production in a continuous inclined rotary reactor were studied separately in order to establish the reactor equations. Concerning geometric and hydrodynamic factors, it was demonstrated that both gas and solid flows can be represented as co-current plug flows in the tubular inclined reactor. Concerning the physicochemical factor, the initial true reaction rate equation had been previously determined and a catalytic deactivation study was performed in a discontinuous reactor, determining that the catalyst follows a sigmoid decreasing law during carbon nanotube growth. Finally, the study of the physical factor highlighted the fact that diffusion of ethylene occurs much faster than the chemical reaction and that ethylene diffusion though the catalytic bed is not the limiting factor. Therefore, it can be concluded that no problem of mass transfer occurred in the continuous reactor.

Once the four factors governing the reactor process were known, the reactor equations could be written. So the modeling of carbon nanotube production in a continuous inclined rotary reactor was performed, applying the co-current plug-flow hypothesis and taking the true kinetic equation and the sigmoid catalytic deactivation into account. The reactor modeling allowed to obtain partial pressure, carbon nanotube production and catalytic deactivation profiles through the reactor. The comparison between the experimental and the calculated productivity showed that the calculated data fitted very well with the experimental data, and that the modeling was in agreement with the experiments.

Acknowledgments

S.L. Pirard is grateful to the National Funds for Scientific Research, Belgium (FNRS) for a Ph.D. grant. The authors also thank the Belgian Fonds pour la Recherche Fondamentale Collective (FRFC), the Région Wallonne - Direction Générale des Technologies, de la Recherche et de l'Énergie, the Ministère de la Communauté Française - Direction de la Recherche Scientifique, the Fonds de Bay and the Interuniversity Attraction Poles Program - Belgian State - Belgian Science Policy - P6/17 for their financial support. The involvement of the University of Liège in the Network of Excellence FAME of the European Union Sixth Framework program is also acknowledged.

Notation

$\underline{a}$ = parameter of catalytic deactivation, s
a = dimensionless parameter of catalytic deactivation
A = pre-exponential kinetic constant, $kmol_{C2H4}.s^{-1}.kg_{catalyst.}^{-1}.atm^{-1}$
$\underline{b}$ = parameter of catalytic deactivation, s^{-1}
b = dimensionless parameter of catalytic deactivation
C_s = total concentration at the external catalytic bed surface, $kmol.m^{-3}$
$\underline{d}$ = parameter of catalytic deactivation, s^{-1}
d = dimensionless parameter of catalytic deactivation
d_b = thickness of the catalytic bed, m
d_r = diameter of the reactor, m
D_e = effective diffusivity, $m^2.s^{-1}$
D_L = axial diffusivity, $m^2.s^{-1}$
D_m = molecular diffusivity, $m^2.s^{-1}$
ΔH° = standard adsorption enthalpy of ethylene, $kJ.kmol^{-1}$
ΔS° = standard adsorption entropy of ethylene, $kJ.kmol^{-1}.K^{-1}$
E_a = activation energy, $kJ.kmol^{-1}$
$\underline{F}$ = total gas flow rate, $kmol.s^{-1}$
$\overline{F}$ = dimensionless total gas flow rate, $kg_{carbon}.kg_{catalyst}^{-1}$
$\underline{F}_{C_mH_n}$ = hydrocarbon flow rate, $kmol.s^{-1}$
$\overline{F}_{C_mH_n}$ = dimensionless hydrocarbon flow rate, $kg_{carbon}.kg_{catalyst}^{-1}$
$\underline{F}_{C_2H_4}$ = ethylene flow rate, $kmol.s^{-1}$
$\overline{F}_{C_2H_4}$ = dimensionless ethylene flow rate
F_{H_2} = hydrogen flow rate, $kmol.s^{-1}$
F_{N_2} = nitrogen flow rate, $kmol.s^{-1}$
k = kinetic rate constant, $kmol_{C2H4}.s^{-1}.kg_{catalyst.}^{-1}.atm^{-1}$
L = length of the useful part of the reactor, m
M = molecular weight, $kg.kmol^{-1}$
M_i = molecular weight of component i, $kg.kmol^{-1}$
m = dimensionless active mass of catalyst
$\dot{m}_C$ = carbon flow rate, $kg.s^{-1}$
$\overline{\dot{m}}_C$ = dimensionless carbon flow rate, $kg_{carbon}.kg_{catalyst}^{-1}$

$\overline{\dot{m}}_{C,e}$ = experimental dimensionless carbon flow rate, $kg_{carbon}.\ kg^{-1}_{catalyst}$
$\overline{\dot{m}}_{C,m}$ = dimensionless carbon flow rate calculated using model, $kg_{carbon}.kg^{-1}_{catalyst}$
$\dot{m}_s$ = catalyst flow rate, $kg.s^{-1}$
M_C = atomic mass of carbon, $kg.kmol^{-1}$
$P_{C_2H_4}$ = ethylene partial pressure, atm
Pe = dimensionless Peclet number
P_{H_2} = hydrogen partial pressure, atm
$\underline{r}$ = specific reaction rate, $kmol_{C2H4}.s^{-1}.kg^{-1}_{catalyst}$
r = dimensionless specific reaction rate
r_0 = initial specific reaction rate, $kmol_{C2H4}.s^{-1}.kg^{-1}_{catalyst}$
r_a = apparent specific reaction rate, $kmol_{C2H4}.s^{-1}.kg^{-1}_{catalyst}$
r_m = specific reaction rate for an ethylene partial pressure equal to 1 atm, $kmol_{C2H4}.s^{-1}.kg^{-1}_{catalyst}$
r_s = specific reaction rate with external catalytic bed surface conditions, $kmol_{C2H4}.s^{-1}.kg^{-1}_{catalyst}$
R = gas constant, $kJ.kmol^{-1}.K^{-1}$
Re = dimensionless Reynolds number
t = time, s
T = temperature, K
u = total gas velocity, $m.s^{-1}$
u_s = average catalyst velocity in the reactor, $m.s^{-1}$
V_M = gas molar volume, $m^3.kmol^{-1}$
x_i = molar fraction of component i
$\underline{z}$ = longitudinal variable in the reactor, m
z = dimensionless longitudinal variable in the reactor
ε = void fraction of catalytic bed
η_s = effectiveness factor
μ = dynamic viscosity, Pa.s
μ_i = dynamic viscosity of component I, Pa.s
ν = kinematic viscosity, $m^2.s^{-1}$
ν_C = stoichiometric factor of carbon
$\nu_{C_mH_n}$ = stoichiometric factor of hydrocarbon
ν_{H_2} = stoichiometric factor of hydrogen
ρ = specific mass of catalytic bed, $kg.m^{-3}$
ρ_g = density of gas, $kg.m^{-3}$
σ = diameter of collision, Å
τ = dimensionless residence time of solid
τ_p = tortuosity factor for catalyst
φ_s = Thiele modulus
Ω_μ = integral of collision

Literature Cited

1. Paradise M, Goswami T. Carbon nanotubes - production and industrial applications. *Mat Des*. 2007;28:1477–1489.
2. Dai H, Rinzler AG, Nikolaev P, Thess A, Colbert DT, Smalley RE. Single-wall nanotubes produced by metal-catalyzed disproportionation of carbon monoxide. *Chem Phys Lett*. 1996;260:471–475.
3. Colomer JF, Bister G, Willems I, Konya Z, Fonseca A, Van Tendeloo G, Nagy JB. Synthesis of single-walled carbon nanotubes by catalytic decomposition of hydrocarbons. *Chem Commun*. 1999;14:1343–1344.
4. Thayer AM. Carbon nanotubes by the metric tons. *Chem Eng News*. 2007;85(46):29–35.
5. Pirard JP. Made in Belgium. *Chem Eng News*. 2008;86(12):5–5.
6. Anonymous. Arkema inaugurates carbon nanotube pilot plant; other CNT developments. *Additives for Polymers*. 2006;2006:6–7.
7. Anonymous. Arkema opens carbon nanotube pilot plant. *Plast Addit Compound*. 2006;8:11.
8. Patent WO 2004/069742, EP1594802B1.
9. Villermeaux J. *Génie de la réaction chimique - Conception et fonctionnement des réacteurs*. Paris: Lavoisier; 1993.
10. Gommes C, Blacher S, Bossuot C, Marchot P, Nagy JB, Pirard JP. Influence of the operating conditions on the production rate of multi-walled carbon nanotubes in a CVD reactor. *Carbon*. 2004;42:1473–1482.
11. Tran KY, Heinrichs B, Colomer J-F, Pirard J-P, Lambert S. Carbon nanotube synthesis by the ethylene chemical catalytic vapour deposition (CCVD) process on Fe, Co, and Fe-Co/Al_2O_3 sol-gel catalysts. *Appl Catal A: General*. 2007;318:63–69.
12. Pirard SL, Douven S, Bossuot C, Heyen G, Pirard JP. A kinetic study of multi-walled carbon nanotube synthesis by catalytic chemical vapour deposition using a Fe-Co/Al_2O_3 catalyst. *Carbon*. 2007;45:1167–1175.
13. Pirard SL, Douven S, Pirard J-P. Analysis of kinetic models of multi-walled CNT synthesis. *Carbon*. 2007;45:3050–3052.
14. Froment G, Bischoff K. *Chemical reactor analysis and design*. New-York: Wiley; 1979.
15. Landau LD, Lifshitz EM. *Fluid mechanics*: Oxford: Butterworth-Heinemann; 1959:6.
16. Satterfield C. *Mass transfer in heterogeneous catalysis*. Cambridge: MIT Press; 1970.
17. Pirard SL, Lumay G, Vandewalle N, Pirard JP. Motion of carbon nanotubes in a rotating drum: the dynamic angle of repose and a bed behavior diagram. *Chem Eng J*. 2009;146:143–147.
18. Kohav T, Richardson JT, Luss D. Axial dispersion of solid particles in a continuous rotary kiln. *AIChE J*. 1995;41:2465–2475.
19. Kuwana K, Endo H, Saito K, Qian D, Andrews R, Grulke EA. Catalyst deactivation in CVD synthesis of carbon nanotubes. *Carbon*. 2005;43:253–260.
20. Wasel W, Kuwana K, Reilly PTA, Saito K. Experimental characterization of the role of hydrogen in CVD synthesis of MWCNTs. *Carbon*. 2007;45:833–8.
21. Bird R, Stewart W, Lightfoot E. *Transport phenomena*. New York: Wiley; 1962.

Manuscript received May 7, 2008, and revision received Oct. 7, 2008.